The Local Analysis and Prediction System (LAPS): Analyses of Clouds, Precipitation, and Temperature

by

Steven C. Albers*, John A. McGinley, Daniel L. Birkenheuer*, John R. Smart

NOAA Forecast Systems Laboratory
Boulder, Colorado

---

* Joint collaboration with the Cooperative Institute for Research in the Atmosphere, Colorado State University, Fort Collins, CO.

Corresponding author address: Steven C. Albers, Forecast Systems Laboratory, NOAA/FSL, R/E/FS1, 325 Broadway, Boulder CO 80303-3328, E-mail: albers@fsl.noaa.gov.

ABSTRACT

The Local Analysis and Prediction System (LAPS) combines numerous data sources into a set of analyses and forecasts on a 10-km grid with high temporal resolution. To arrive at an analysis of cloud cover, several input analyses are combined with surface aviation observations (SAOs) and pilot reports of cloud layers. These input analyses are: a skin temperature analysis (used to solve for cloud layer heights and coverage) derived from Geostationary Operational Environmental Satellite (GOES) IR 11.24 μm data, other visible and multispectral imagery, a three-dimensional temperature analysis, and a three-dimensional radar reflectivity analysis derived from full volumetric radar data. Use of a model first guess for clouds is currently being phased in. The goal is to combine the data sources to take advantage of their strengths, thereby automating the synthesis similar to that of a human forecaster.

The design of the analysis procedures and output displays focuses on forecaster utility. A number of derived fields are calculated including cloud type, liquid water content, ice content, and icing severity; as well as precipitation type, concentration, and accumulation. Results from validating the cloud fields against independent data obtained during the Winter Icing and Storms Project (WISP) will be presented.

Forecasters can now make use of these analyses in a variety of situations, such as depicting sky cover and radiation characteristics over a region, three-dimensionally delineating visibility and icing conditions for aviation, depicting precipitation type, rain and snow accumulation, etc.

1. Introduction

New data sources available at NOAA's Forecast Systems Laboratory (FSL) are being applied to develop new types of mesoscale analyses. LAPS (McGinley 1995) produces analyses with an adjustable grid resolution, nominally 10 km horizontally and 50 hPa vertically. The local FSL domain currently covers northeastern Colorado as well as parts of adjoining states to the north, east, and south. LAPS analyses of temperature, moisture, pressure, winds, and clouds are being developed. This report focuses on the analyses of clouds and other hydrometeors, as well as temperature, an important input. Most fields from these analyses are examined on meteorological workstations at FSL and at other field locations with locally established domains.

The datasets ingested in real time are representative of the data networks of the future, and present a unique opportunity to develop operational local assimilation and processing systems that can cope with new high-volume data sources. New methods of fusing the disparate data sources, taking into account the strengths of each source, will greatly enhance the mesoscale analyses that are performed. This is distinct from previous works (e.g. Hamill et al. 1992) which produced analyzed cloud fields with a more limited set of input data (mostly polar orbiting satellite and SAOs). The unique features of the LAPS cloud analyses include combining data sources like surface observations, satellites, pilot reports, and radar data to provide a more complete three-dimensional view of clouds. The use of geostationary satellite data helps provide for high temporal resolution (satellite data arrive every 15 minutes) and broad areal coverage (potentially an entire hemisphere), consistent with high spatial resolution (10-km horizontal and as small as 100-m vertical). Another cloud analysis scheme (Schiffer and Rossow, 1985) supports the International Satellite Cloud Climatology Project (ISCCP). This analysis uses multiple satellites, though it operates on a larger scale (250-km with a 3-h update cycle). ISCCP uses a different approach to calibrate the visible satellite data than LAPS. They also have different approaches for analyzing cloud optical depth and cloud droplet size. We are currently phasing in the use of a model first guess to provide additional information. The LAPS cloud analysis is designed to maximize consistency with all input data as well as the typical meteorology of clouds.

The three-dimensional LAPS analyses discussed in this report include cloud coverage, temperature, and radar reflectivity. Liquid water equivalent precipitation and snow accumulation along with precipitation type and concentration are derived from the radar reflectivity, temperature, and moisture analyses. Fields derived primarily from the cloud analysis include cloud liquid water (both three-dimensional and vertically integrated), cloud type, cloud droplet size, and icing severity. The cloud fields are inputs for the LAPS humidity analysis and are used to aid initialization of the forecast modeling component of LAPS.

The resulting local high-resolution, gridded analyses will be a valuable resource within the Weather Forecast Office (WFO). They allow forecasters to quickly update their knowledge of the structure of local fields, animate these fields on a workstation, diagnose nonstandard quantities, and interact with the database to develop new forecast products and methods.

These advancements will help the weather services meet the goal of improved forecasts in the 0-6 h period.

2. Datasets used in LAPS

FSL has supported a unique, data rich environment for many years. Doppler radar, wind profiler, thermodynamic radiometers, and surface mesonet data flow into the database 24 hours a day. The data collected routinely include the following:

- Surface observations at 22 local sites every 5 min, as well as hourly SAOs from North America.
- Doppler radar volume scans at 6-min intervals.
- Wind and temperature Radio Acoustic Sounding System (RASS) profiles from the NOAA Demonstration Profiler Network (60-min interval).
- Satellite visible data (30-min interval) and multispectral image and sounding radiance data (90-min interval).
- Automated and voice reports from selected aircraft at random times.

These data are roughly comparable to what will be available at most Weather Forecast Offices (WFOs) by the late 1990s. We can conservatively expect that within a 300-km radius of most WFOs, there will be 8-15 SAOs and Automated Surface Observing Systems (ASOS), a Doppler radar (some locations will have two), one or more wind profilers, aircraft observations, and a variety of satellite data. Thus we have designed a data assimilation and analysis system compatible with this data configuration.

Most LAPS fields reside in a 10-km horizontal, 50-hPa vertical, 61 x 61 x 21 grid, and are now being produced in real time at 60-min intervals. The cloud cover analysis (shown in Figure 1) is performed on a higher resolution height grid (42 vertical levels). This grid has approximately 100 m grid spacing near the ground, increasing to about 1000 m near the tropopause.

3. Three-Dimensional Temperature Analysis

The LAPS three-dimensional temperature analysis is produced using a blend of FSL's Mesoscale Analysis and Prediction System (MAPS) model (Bleck and Benjamin 1993), RASS (and rawinsonde / dropsonde) temperatures at upper levels, and the LAPS surface temperature analysis at lower levels. This analysis is an important prerequisite to the cloud analysis, since the temperature field is used in conjunction with satellite-derived brightness temperatures.

The LAPS surface temperature analysis is part of a complete set of surface analyses generated hourly (McGinley et al. 1991). All the standard meteorological variables, as well

as several diagnostic derived variables, are routinely analyzed. A variational procedure is used to dynamically adjust the wind and pressure fields with other specialized techniques, such as allowing the high-resolution terrain information to influence the temperature field, being included in the analysis package. For surface temperature, observations within the LAPS domain are analyzed using a smooth, one-pass Barnes (1964) analysis, and a simple quality control procedure removes data that exceed a representative number of standard deviations from the analyzed value. A two-pass Barnes analysis is then used to define the boundaries, and a cubic spline matches the interior of the grid to the observations.

The upper-level temperature field is interpolated four dimensionally from the MAPS analyses and forecasts produced at FSL. Next, vertical temperature profiles from the sonde and RASS data are inserted if available. The surface temperature analysis is inserted as a final step, providing information for the lower levels of the three-dimensional temperature analysis. The RASS, sonde, and surface data provide forecasters with an updated look at the evolution of the boundary layer over varying terrain, especially when the temperature field is viewed in cross section (Figure 2).

a. *Insertion of temperature sounding data*

Hourly averages of RASS vertical temperature sounding data ending at the LAPS analysis time are used with other temperature soundings obtained during the hour. The RASS soundings are calculated using the raw RASS virtual temperatures combined with specific humidity and pressure/height information from the model first guess data (e.g., MAPS). When one temperature profile is present in the domain, the data are inserted by computing a temperature bias relative to the background field at each level. This bias is then added to all grid points in the background field at the current level. The LAPS domain is generally small enough in horizontal extent that the explicit application of a radius of influence in this step may create excessive horizontal temperature gradients, hence the constant bias is added to the background over the entire horizontal extent of the domain. Above the top level where temperature data are present (typically $\sim$550 hPa in the case of RASS), an additional level with half the bias of the top sounding level is added to smooth the vertical discontinuity of the sounding insertion. Below the lowest sounding level (500 m AGL for RASS), the bias is set to the bias at the lowest sounding level.

If multiple temperature profiles are present, the biases are analyzed with a Barnes analysis, which is configured with a spatially varying radius of influence to account for clustering of observations. This follows the procedure for the Barnes analysis used for LAPS winds (Albers 1995). At each level, the biases are analyzed and the resulting analysis is what becomes added to the background.

Several quality control checks are applied to the biases. For example, if the magnitude of the bias exceeds 10 degrees at any level, the entire profile is assumed to be bad.

b. *Insertion of LAPS surface temperature analysis*

To insert the LAPS surface data, a 50 hPa boundary layer is defined above the local terrain. The bottom of the layer is set to equal surface analysis temperature, and the top is specified by the first guess (MAPS plus temperature soundings) interpolated temperature. Note that the insertion procedure for the surface analysis is carried out only at those grid points whose surface pressure is >750 hPa. Our experience so far has been that the other data sources are generally more accurate at higher altitudes above the elevations of most surface reporting stations.

Within the boundary layer, a correction is phased in by calculating a residual of LAPS surface minus the first guess. The residual is ramped in by adding half the bias in the middle of the boundary layer, the full bias at the surface, etc. This helps preserve the vertical temperature structure of the first guess within the boundary layer while ensuring consistency between the three-dimensional temperature field and the LAPS surface temperature analysis.

If, at a given grid point, the value of potential temperature (θ) exceeds the value at the next higher grid point, the value at the higher grid point is set to the current grid point. This prevents the existence of superadiabatic layers in the final temperature analysis. This upward propagation of temperature corrections is designed to allow surface observations (which are often more up to date and accurate than upper air data, especially during periods of strong insolation) to define the potential temperature of the mixed boundary layer. Those levels just above the surface acquire the same potential temperature as the surface through the correction process.

The LAPS height field is also computed at this point. This computation involves a hydrostatic integration of the temperature field using the LAPS terrain and surface pressure fields as boundary conditions.

4. Radar reflectivity analysis

Radar volume data, also input to the cloud analysis, are available in remapped form on the LAPS grid. During the early 1990s the data were generated on the PROFS real-time Doppler products subsystem (Lipschutz et al. 1989). A program similar to FSL's implementation of many of the Next Generation Radar (NEXRAD, 1985) algorithms ran in real-time, generating three-dimensional cartesian gridded radar data for each volume scan of Mile-High Radar, located 20 km northeast of Denver, Colorado. It employs a V-notch clutter filter that suppresses some of the ground clutter; this remapping algorithm will be modified to operate with the network of WSR-88D radars as they become operational.

A range-unfolding algorithm is employed that compares reflectivities at two different pulse repetition frequencies. In this way, aliased reflectivities on the short-range scan can be moved outward to their actual location. For each LAPS grid point, the remapping algorithm computes reflectivity by taking the mean dBZ value of all gates within a grid volume centered on the LAPS grid point. Computer limitations inherent in the FSL Mile-High radar Doppler products subsystem did not allow experimenting with other types of averaging. When the mean reflectivity is less than 0 dBZ, it is set to a flag value of -10

dBZ.

The data are written out in sparse byte arrays, which allows disk-space savings between one and two orders of magnitude. A subroutine reads the packed radar files and decompresses the radar data. The radar reading subroutine has the option to apply a three-dimensional ground clutter map to the reflectivity data. This fixed clutter map resides in the LAPS grid and consists of the maximum reflectivity in each LAPS grid volume from several clear-air volume scans. When the clutter map is applied, any observed reflectivity not exceeding the clutter map by 10 dBZ is set to the base value of -10 dBZ (no meteorological echo).

The volumetric coverage of reflectivity data must also pass a temporal continuity test. If the number of valid reflectivity gates differs by more than a preset threshold between successive volume scans, the later scan is flagged as bad. A single bad volume scan (often occurring near startup) may thus cause two successive scans to be flagged as bad. An additional subroutine fills in gaps of up to three vertical levels using linear interpolation. This is to allow for the space between successive radar sweeps with increasing antenna elevation. This routine also has the option of filling in echo in low levels judged to be either below the radar horizon (due to the earth's curvature) or masked by mountains or ground clutter. Any echo base within two LAPS grid levels of the local terrain is assumed by the fill routine to extend down to the ground. The appropriate extrapolation is done by extending the reflectivity at the lowest observed level downward to the ground.

Among the fields derived from the radar analysis are echo top height and a 1-h forecast of echo location based on layer mean winds. Layer mean winds are calculated from the surface to 300 hPa as described separately. The echoes for this field are advected with a surface to 300 hPa layer mean wind speed, except near convective storms, where storm-tracking vectors are utilized.

Another way to present radar data involves computing the maximum reflectivity over a given LAPS grid point for the duration of the 1-h analysis cycle. This maximum reflectivity analysis is being utilized in LAPS displays on meteorological workstations at FSL.

The cloud and precipitation analysis package can also operate with reduced capability using two-dimensional radar reflectivities, such as that provided by NOWRAD radar data over the continental United States.

5. Three-Dimensional Cloud Cover Analysis

a. *Overview*

The cloud cover analysis is useful for forecasters in depicting the areal extent of cloud cover under various conditions and for aviation interests concerned with the three-dimensional distribution of clouds. A visible or IR satellite image alone does not provide as complete a rendition of cloud locations. To arrive at an analysis of cloud cover, several input

analyses are combined with SAOs of cloud layers. Figure 3 presents a data-flow diagram for the cloud analysis. The principal input analyses include GOES IR 11.24μm imagery, GOES visible and other multispectral satellite imagery, three-dimensional temperatures, as well as the gridded three-dimensional LAPS radar reflectivity derived from full volumetric radar data.

Vertical cloud "soundings" from SAOs and pilot reports are analyzed horizontally to generate a preliminary three-dimensional analysis. This step provides information on the vertical location and approximate horizontal distribution of cloud layers. Observations over a region slightly larger than the LAPS domain are utilized. The satellite cloud-top temperature field (derived using GOES IR 11.24μm imagery) is converted to a cloud-top height field with the assistance of the LAPS three-dimensional temperature field. The cloud-top height field is then inserted into the preliminary cloud analysis to better define the cloud-top heights and increase the horizontal spatial information content of the cloud analysis. A set of rules is employed to resolve conflicts between SAO and satellite data. The SAO data dominate the analysis of low or warm clouds. For higher clouds, the SAO data provide the potential location of the vertical layers. The coverage of the layers is controlled by the satellite data. The coverage of the cloud layers is adjusted as needed to ensure consistency between derived analysis and measured infrared brightness temperatures.

The three-dimensional radar reflectivity field is next inserted to provide additional detail in the analysis. Finally, visible satellite data are inserted if available. Note that the order of processing helps determine the relative influence of the various data sources. The satellite data are inserted for each grid point after the SAO data even at those grid points closest to the SAO location. Despite the potential for the satellite (and radar) data to cause the final analysis to differ slightly from the SAO data, the agreement turns out to be satisfactory. Detailed comparison of this agreement provides a good quasi-independent check on the methodology used to insert the satellite data, both at and between the SAO locations. This comparison also allows fine tuning of the relationship between SAO sky cover and the cloud fraction values used in the SAO-derived soundings. Figure 4 illustrates a cross section through the three-dimensional gridded LAPS cloud field.

Cloud cover is defined in the analysis at each of the vertical height levels. If a cloud layer is determined to have a density of d, where density represents the cloud layer's opacity to visible or infra-red radiation, then the cloud cover at each contiguous vertical grid level within the cloud layer is assigned a cloud cover numerically equal to d.

b. *Analysis of SAO and aircraft data*

For every SAO location, a vertical profile of cloud fraction is generated. This is schematically shown in Fig. 5 in the form of arrows extending upward from each of three SAO stations. Solid bars indicate levels where cloud is regarded as existing. These vertical profiles are mapped onto the vertical LAPS grid as column vectors and then spread horizontally through the three-dimensional LAPS grid. The cloud grid has more vertical levels than other LAPS grids, with 100 m height resolution at low levels up to 1000 m at

high levels. If a cloud ceiling is found in the SAO, an assumed thickness then specifies the cloud-top height. The value is somewhat dependent on the altitude of the cloud, but is generally 1000 m. This thickness becomes the final cloud thickness if no other data intervenes (e.g. satellite, model first guess) at a later stage of processing. The values used are derived from visual observations of clouds by the authors. For that station, grid points above the overcast layer are not initialized because the cloud profile is unknown. The uninitialized portions of the cloud sounding do not weigh into the objective analysis of clouds at that location. ASOS observations are used just as reports made by a human observer, but cloud soundings derived from them also terminate below the top of the LAPS grid (normally about 3700 m above ground level).

A quality control step clears out those cloud layers or parts of layers existing within a temperature inversion if the ambient temperature exceeds 283 K and the value of theta exceeds that at ground level by 4 K. This step appears to produce a better analysis when the SAO is implying cloud layers present within a low level inversion where the implied mixing ratio in the warm dry air aloft would be excessive.

Cloud bases, tops, and layers defined by pilot reports are also inserted. If just a base is given, an assumed cloud layer 1000 m thick is initialized and a clear buffer of 500 m is inserted below the cloud base. The same is true for having only a cloud top, except the assumed layer thickness is 500 m. If a complete layer is specified in the pilot report, the layer is given 100% cloud cover and a 500 m buffer of 0% cover above and below. These values seem reasonable based on visual cloud observations. Once the data are inserted, horizontal objective analysis on the sparse grid is performed to generate a continuous cloud field. The weight given to each station is proportional to (r^{-5}) where r is the distance of the station from the grid point being analyzed. This guarantees that the analysis almost exactly matches the observations at the station locations.

c. *Insertion of infrared satellite data*

Infrared satellite data at 11.24μm is first used in a selective deletion process that supplies more horizontal structure to the cloud field generated by the SAO and aircraft data. The brightness temperature measured by the satellite is compared with the "expected" clear sky brightness temperature calculated using the preliminary analysis built from SAO and aircraft data. Cloud coverage and ground temperature are taken into account.

The ground temperature (given clear skies) is specified by the LAPS surface analyzed air temperature as a first guess. It is then refined using an empirical model to estimate its deviation from the air temperature by including a function of the solar elevation angle, declination, and hour angle. This deviation reaches approximately +4 K during the day and -4 K during the night. The deviation crosses the zero point at approximately those times during the day of air temperature extrema. Snow cover information provides a further refinement. When snow is present, the ground temperature is not allowed to exceed either the air temperature or 273 K. This model appears to reduce the standard

deviation between calculated ground temperature and 11.24μm brightness temperatures for clear sky cases.

Here it is assumed that the expected brightness temperature is a weighted composite of the cloud-top temperature and the ground temperature taking into account the density of the cloud layer. For each vertical level, if the measured 11.24 μm brightness temperature is greater than the expected temperature, the cloud cover and density of the level is reduced to be consistent with the observed brightness temperature. To prevent erroneous clearing of very low cloud decks, clouds lower than 800 m AGL or clouds having a temperature within 10 K of the surface air temperature are excluded from the deletion procedure. This allows the SAO and aircraft data to dominate in the analysis of those clouds too low or warm to have a cold infrared signature.

Cloud-top heights are being specified by the 11.24 μm IR data and the temperature field. Brightness temperatures at 11.24 μm are compared to the temperature analysis, and the lowest level at which there is a match becomes the satellite-derived cloud top. At this stage in the processing, the cloud top is assumed to be optically thick. The satellite-derived cloud tops are inserted into the cloud field by employing an additive process. In this step, clouds may be added over the top of existing SAO and aircraft data-derived cloud decks or, if relatively high, they are created solely on the basis of the satellite data.

For each horizontal grid point, the presence of cloud is flagged when the IR brightness temperature is more than 8 K colder than the ground temperature. This allows some slack for various error sources in the IR brightness temperature and the LAPS analyzed surface temperature, preventing false cloud detections.

The 8 K tolerance check provides that satellite-implied clouds will not be indicated below 800 m AGL given a nearly dry adiabatic lapse rate. Once again, this allows analyzed clouds below 800 m AGL to be controlled strictly by SAO and aircraft data. This is important in preventing false detections in very low clouds.

In the normal case, a cloud is analyzed with a cloud top equalling the satellite derived cloud top and whose thickness equals a default thickness of 1500 m. The cloud cover throughout the analyzed layer is set to 1. If the IR cloud base extends below an existing analyzed SAO and aircraft data cloud base, the base is adjusted upward to equal the SAO and aircraft data analyzed base. If this adjustment is made for a cloud top derived from 11.24 μm data, then a reduced value for the cloud cover is calculated to be consistent with the observed brightness temperature. We again assume that the apparent brightness temperature is a weighted composite of the cloud top temperature and the ground temperature. The weights are determined by the cloud fraction of the layer.

d. *Conflicts of SAO and aircraft data with IR data*

Generally, the cloud tops given by the IR data are consistent with the cloud bases and layers given by the SAOs and aircraft data analysis. There are exceptions, however, and several error checks are required to handle those situations.

1) If the IR cloud tops are lower than the lowest SAO and aircraft data cloud base, they are reset to equal the lowest SAO and aircraft data cloud base plus the default cloud thickness.

2) If the IR indicates cloud but no nearby SAO and aircraft data cloud layers are present, the indicated cloud layer must be colder than the ground by 21 K or be located above 5000 m AGL; otherwise no cloud is analyzed.

3) Tests are being performed to check the consistency of the cloud layers and cloud fractions with the satellite 11.24 μm brightness temperature. The calculated radiance using the cloud analysis is compared to the measured satellite radiance. This diagnostic tool has helped to point the way to a number of recent improvements in the analysis. Examples include better placement of the edges of low stratus decks and better detection of isolated (e.g., mountain wave) clouds. In these cases, performing the analysis is more difficult because the clouds are not necessarily seen by the nearest SAO station.

4) A corrective scheme is being employed to modify the cloud cover field so as to better satisfy the 11.24 μm consistency test. It operates by iteratively adding the same value to the cloud cover in all layers visible to the satellite. This correction parameter is adjusted until the consistency test reaches an optimum match.

e. *Insertion of Radar Data*

A radar echo is treated as a region of cloud as long as it is above the lowest cloud base indicated by the SAO and aircraft data analysis. A dBZ threshold is used: 5 dBZ if the ambient temperature is $<282K$, or 20 dBZ if it is $>282K$).

Quality control checks are performed to compare the radar data with other data sources. If the rest of the cloud analysis indicates no cloud, but the radar indicates echo at a particular horizontal grid point, the radar echo is generally assumed to be spurious. If the reflectivity >10 dBZ and the visible satellite data indicate a cloud cover < 0.2, then the visible data (Sec 5f) is modified to indicate a cloud fraction of 0.2. These checks are sufficient to ensure perfect consistency between the three-dimensional cloud and radar fields, at least in the horizontal dimensions. The three-dimensional consistency is also improved to an acceptable level.

f. *Insertion of Visible Satellite Data*

Visible satellite data insertion, the final processing step, can be used wherever the solar elevation angle is >15 degrees. GOES visible satellite data are remapped by averaging onto the LAPS domain. The brightness values are then normalized according to the viewing and illumination geometry according to Albers (1992). This provides a uniformly illuminated dataset that can be calibrated in terms of albedo and cloud cover. The cloud cover for each LAPS grid column is reduced to that derived by the visible satellite if it is significantly lower. The main benefits of visible data are higher resolution, increased delineation of clear areas in low cloud decks, and rendition of thin clouds. Perhaps in

the future, the information on thin clouds can be used to adjust cloud-top heights using infrared temperatures that are not representative of actual cloud top temperatures.

6. Three-dimensional Cloud Type Algorithm

Cloud type is defined as a function of ambient temperature and $\partial\theta_e/\partial z$, the vertical gradient of equivalent potential temperature (Table 1). The θ_e field is calculated using the LAPS three-dimensional temperature field but assuming saturated conditions within the cloud. Stability is calculated using centered θ_e differences. Cloud type is calculated in regions where the cloud cover fraction exceeds 0.65. In table 1, cloud type and mean volumetric drop (MVD) size are calculated using a two-dimensional matrix, with ambient temperature and $\partial\theta_e/\partial z$ as input. For each category, the cloud type and MVD are specified. The values of MVD are those used by the Smith-Feddes method (Haines et al. 1989). A data-flow diagram for these derived fields appears in Fig. 6.

a. *Cloud omega field*

A cloud omega field is derived from the cloud locations and type. The derived omega field is a function of cloud type and depth. A constant value (.05 m s^{-1}) is used within stratiform clouds, and parabolic vertical profiles are used in cumuliform clouds. The empirical parabolic function has an amplitude proportional to cloud depth, reaches a peak one-third of the way up from the base, and extends below the cloud base by one-third of the cloud depth. The cloud omega field is undefined outside of cloudy areas. This field is used to fine-tune vertical motion and divergence fields within LAPS, specifically for the forecast model initialization, described later (Sec 9a).

7. Three-dimensional cloud liquid water/ice algorithm

Cloud liquid water (both three-dimensional and vertically integrated) is calculated in LAPS in regions where the cloud cover fraction exceeds 0.65. This method involves adapting the Smith-Feddes model (Haines et al. 1989) to run in the LAPS three-dimensional environment instead of with soundings (McGinley and Albers, 1991). Here, we essentially treat each column of grid points in the LAPS domain as a sounding and run the Smith-Feddes model on it. Stratus clouds are assumed for input to the Smith-Feddes model. An empirical depletion due to ice nucleation is applied to the liquid water values as a function of ambient temperature at the level being considered. This is done because the Smith-Feddes model, when used operationally, produces excessively high values of liquid water below $-20°C$. The original Smith-Feddes model appears to treat cold ambient temperatures in stratus clouds only through a calculation of the probability of clouds having ice. This was not directly used in LAPS.

A concise updated version of this algorithm (personal communication with Haines 1992) is what we are using in LAPS for layers whose cloud cover exceeds 0.65. This algorithm also employs an empirical depletion of cloud liquid based on ambient temperature; it is transformed into cloud ice such that LAPS now produces three-dimensional concentrations of cloud liquid and cloud ice. In the future, we may revisit the question of whether

the depletion of cloud liquid results in cloud ice or precipitation sized ice particles.

Doppler radar, one of the sources of data ingested by LAPS, provides a fairly direct measure of the precipitation falling within the domain, given that one can arrive at an estimate of the type and size spectrum of the precipitate. A comparison of LAPS radar reflectivity with the liquid water content measured from a research aircraft reveals (for non-convective situations) a threshold near 10 dBZ, above which no liquid water is detected. This suggests a more direct method of adjusting calculated liquid water content (LWC) to account for depletion by ice or, more correctly, precipitate. This depletion scheme is included as the last stage of the LWC calculation.

If the cloud cover is less than 0.65, then cloud liquid and ice are calculated using assumptions about the cloud optical depth and drop size. For these thin clouds, one can approximate the cloud optical depth τ by setting it to the density of the layer or maximum analyzed cloud cover within the layer. Using the total optical depth and thickness ds of the layer, we divide the two yielding a scattering coefficient σ; this equates to knowing how much scattering or obscuration occurs per unit depth in the layer.

$$\sigma = \frac{\tau}{ds} \tag{1}$$

Assuming that the diameter D of the cloud water/ice particles is 20 μm (and that the geometrical area of a particle equals its scattering cross section), we solve for the number density N of the cloud particles as follows.

$$N = \frac{\sigma}{\pi(0.5D)^2} \tag{2}$$

The number density N and mean particle diameter D are then used to solve for the specific content or cloud water/ice mixing ratio. The relative amount of each phase ramps linearly between ambient temperatures of $263.15K$ and $243.15K$.

a. *Icing severity and verification of LAPS LWC against aircraft data*

Supercooled LWC is derived for each LAPS grid point, as explained above. The operational version utilizing the Smith-Feddes algorithm is used. The icing severity is given by the supercooled LWC.

We have performed comparisons of LAPS cloud liquid water against WISP-90/91 research aircraft LWC measurements (Rasmussen et al. 1991). Aircraft measurements are averaged with a smoother that applies a 100-sec running mean. This is about the time it takes for the aircraft to traverse a LAPS grid box, thus suppressing subgrid-scale variability in the observed liquid water. Small-scale variability (on a scale slightly larger than the LAPS grid resolution of 10 km) in the field is not fully resolved by LAPS and accounts for much of the scatter observed in point comparisons (Fig. 7). This comparison

is a very sensitive end-to-end test of the LAPS analyses and must be interpreted in light of expected results using other analysis and modeling schemes.

It is noteworthy that most of the points lie near or below the main diagonal on the plot. This demonstrates that LAPS has significant skill in predicting an upper limit of liquid water likely to be encountered by an aircraft. The absence of data points near the y-axis is a strong nonrandom signature representative of a very high probability of detection. Both the small-scale, three-dimensional placement of clouds and the diagnosis of liquid water in these clouds affect the comparisons. The relatively high resolution of the analysis suggests that LAPS can reduce the false alarm rate over icing forecast schemes that operate in the large scale simply by delineating where clouds are absent on the small-scale. We can thus surmise that the critical success index (CSI), Donaldson et al. (1975), is relatively high in the LAPS liquid water field.

Additional validation of LAPS icing severity was performed against commercial aircraft icing reports (Mahoney et. al. 1995). This study shows a favorable comparison of LAPS against a relatively small sample of point aircraft icing reports. Validation of the LAPS liquid water on independent WISP data was done at a larger spatial scale in McGinley and Albers 1991. In this study, the performance of LAPS compared favorably to simply using nearby sounding data.

8. Precipitation type and snow/liquid accumulation/concentration

a. *Diagnosis of precipitate type*

A three-dimensional precipitate type field helps to specify the hydrometeors present in the LAPS domain. The precipitation analyses are useful for forecasters in depicting the areal extent and type of precipitation and for aviation interests concerned with the three-dimensional distribution of hydrometeors. Radar or surface observations alone do not provide as complete a rendition of the three-dimensional hydrometeor distribution. The input fields are radar reflectivity and wet-bulb temperature. The possible diagnosed precipitate types are: no precipitate, rain, snow, freezing rain, sleet, and hail. The LAPS radar reflectivity must exceed 0 dBZ to declare precipitate as being present.

A one-dimensional steady-state model utilizes temperature and radar data in each vertical grid column. Precipitate begins as snow if the echo top is in air colder than $0°C$, otherwise it starts as rain. Wet-bulb temperature is used instead of dry-bulb as this more accurately estimates the temperature at the surface of a hydrometeor. A good example is when snow falls in dry air with a dry-bulb temperature exceeding $5°C$. In this case, evaporative cooling is an important reason the snow may not melt.

As we track the precipitate downward through the radar echo, if the ambient wet-bulb temperature is $>1.3°C$, the precipitate melts to rain. This melting threshold is slightly above $0°C$ to account for the time lag for snow to completely melt. The specific number used gives the best agreement between LAPS precipitation type and verifying SAOs for a two-month period in fall 1994 over the Colorado LAPS domain.

If the precipitate once again falls into a layer $<0°C$, it becomes freezing rain. A time lag is considered for the subsequent refreezing of rain to sleet. The criterion for refreezing is a subfreezing layer having a depth (where the Celsius wet-bulb temperature is integrated over pressure) of -25000 $Pa -° C$. An example would be a layer 5000 Pa deep with a temperature of $-5°C$.

To diagnose hail, a simple threshold of >45 dBZ radar reflectivity is used. The LAPS radar analysis smooths the raw high-resolution radar data to the 10-km LAPS grid, thus reducing peak reflectivities in small-scale convective storms. Given this effect, 45 dBZ within the LAPS analysis represents a significant convective storm.

A two-dimensional surface precipitation type field is derived from the three-dimensional field as follows. A simple extraction from the three-dimensional field is done to create a preliminary two-dimensional analysis. At each grid point, the pressure level used is the one closest to the surface pressure or the one immediately above, depending on the circumstances. The preliminary analysis is refined by considering the surface wet-bulb temperature field derived from LAPS surface temperature and dewpoint analyses. This helps correct slight interpolation errors.

A further option exists for display of the surface precipitation type on meteorological workstations involving thresholding based on additional meteorological data. A low-level reflectivity threshold is set to 0 dBZ for snow and 13 dBZ for nonsnow precipitation (translating roughly to what is often considered as measurable precipitaton over a 1-h period). Below this threshold, the surface precipitation type is set to no precipitation - mainly so that very light rainfall is not displayed. In the event that LAPS is using single level (NOWRAD) radar reflectivity as input, surface dewpoint depression (when $>10K$) is used to deassign areas of snow, covering situations where virga is considered likely. Areas having no detected radar echo are assigned precipitation type based on surface precipitation observations at the nearest SAO station as well as cloud cover at the grid point in question for rain, snow, drizzle, and freezing drizzle. This accounts for cases when precipitation is either too weak to be seen on radar or beyond radar range.

Figure 8 shows an example of the precipitation type analysis on 14 February 1995 at 2100 UTC. This event was characterized by low-level upslope (easterly) flow across northeastern Colorado behind a surface cold front which, at that time, was located over southeastern Colorado. Rain (R) is diagnosed close to the front while freezing rain (Z) is the precipitation type diagnosed along the northern Front Range corridor. Enhanced vertical motion near the foothills of the Continental Divide combined with low-level cold advection occassionally creates an atmospheric structure that supports freezing rain or drizzle and snow in local areas over eastern Colorado. That this structure is present in the three dimensional LAPS analysis, combined with detailed knowledge of the distribution of precipitation-sized hydrometeors results in a highly detailed analysis of precipitation type. Over the higher terrain of Colorado the precipitation type is diagnosed as all snow (indicated by asterisks). Meteorologists who live in the Front Range Corridor observed freezing rain and foothills snow at the time of this analysis confirming its accuracy.

b. *Liquid equivalent/snow accumulation fields*

A liquid water equivalent precipitation and snow accumulation algorithm implemented in the LAPS domain utilizes LAPS low-level radar reflectivity and surface precipitation type fields. The snow accumulation is linked to rain accumulation via a rain-snow ratio. This ratio is a function of the column maximum temperature, starting from 10:1 for $T = 0°C$, increasing to a peak of 25:1 for $-18°C < T < -10°C$, and decreasing back to 15:1 for $T < -22°C$. This accommodates approximate ratios observed in varying situations by the authors.

This computation is performed where snow is diagnosed by the surface precipitation type field. The rate is set to zero if either no precipitation is occurring or nonsnow precipitation is diagnosed. The Z-R relationship is currently the Marshall Palmer relationship $Z = 200R^{1.6}$ (R in mm hr^{-1}). The liquid water equivalent precipitation and snowfall rates derived from each radar volume scan are integrated in time to produce incremental and storm total liquid water equivalent precipitation and snow accumulation gridded fields. Figure 9 shows an example of the liquid water equivalent precipitation accumulation field. In this example, the precipitation was convective, thus areas of heavy rain and possible flooding are depicted that may be of concern to forecasters. This field is also useful for verifying forecasts of the areal extent and amount of precipitation.

We have also implemented an approach to generating a precipitate concentration field. This takes the existing Z-R relationship and converts it to precipitate concentration, dividing the precipitation rate by the fall velocity. The fall velocity is a simple function of precipitate type and ambient air density.

c. *Diagnosis of snow cover*

We have implemented a snow cover analysis to be utilized as inputs to ground temperature and soil moisture analyses, as well as the Colorado State University-Regional Atmospheric Modeling System (CSU-RAMS). The fields of column maximum cloud cover, visible satellite albedo and satellite-derived skin temperature are combined to create a fractional snow cover field (CSC), defined at each grid point in areas that are cloud free for that analysis cycle. A grid point is assumed to be cloud free if the column maximum cloud cover is less than 0.1. In these areas, the visible satellite albedo is converted to snow cover using a linear scale. As an additional check, clear areas having brightness temperatures in excess of 281 K are automatically assumed zero snow cover. Intermediate fractions between 0 and 1 represent dirty or patchy snow. The idea is essentially to define snow or no snow for the grid point if possible. A composite field is developed (Cram and Albers 1994) using the CSC field over a 48-hr period to minimize the impact of moving cloudy areas as well as the day/night cycle. This field in turn can be combined with radar-derived snow accumulation and SAO data (i.e., 904 groups) for a more complete snow cover or snow depth product.

9. Two-way forecast model interaction

a. *Initialization of the CSU-RAMS model*

We are using real-time 10-km LAPS moisture analyses to initialize the CSU-RAMS model in twice daily forecast runs at FSL. The model is utilizing input of LAPS specific humidity, cloud water, cloud ice, and surface snow cover. The cloud omega field (Sec 6b) has been used as well in model initialization experiments. These fields were shown to qualitatively improve the depiction of model forecast moisture related fields (Cram et al. 1995a,b; Cram and Albers 1994).

b. *Use of model first guess information*

We are developing strategies for using first guess information from a forecast model in constructing the cloud analysis. This would be especially useful in data-poor regions of the LAPS grid beyond the view of the various sensors (e.g., surface observations).

Our current approach is to use the model specific humidity and temperature fields to calculate relative humidity. We then use this to derive a cloud fraction in the stage where the SAO data are analyzed in the cloud fraction analysis. In those levels where there is no SAO and PIREP defined cloud analyzed (i.e., no SAO cloud soundings occur anywhere in the horizontal domain), the cloud fraction is set equal to the model relative humidity. We plan to modify this to use a more accurate relationship to convert from relative humidity to cloud fraction. We also plan to use a criterion for using the model background when the distance from a particular grid point to the nearest SAO and PIREP defining clouds at the given level exceeds a constant. This approach is relatively conservative, but will be used increasingly in the future.

Another method involves the use of model information that behaves more as a quality control check (as explained in Sec 5b). If a cloud layer is analyzed at low levels, it is compared to the model background vertical temperature profile. If the analysis (at the initial SAO stage) is analyzing a widespread cloud that extends through the top of a significant inversion and the dew point is high, then the cloud top is reduced in height to coincide with the temperature inversion. One possible scenario for this is when the "default thickness" places an assummed cloud top above the inversion level.

10. Future work

a. *Cloudtops derived from CO_2 slicing method*

We are experimenting with the CO_2 slicing method (Wylie and Menzel 1989) (hereafter called the slicing method) to provide a possible improvement to cloud top altitude and cloud amount. This technique utilizes the GOES sounding channels of 14.23 μm, 13.99 μm, 13.31 μm, and 11.24 μm), to solve for cloud top pressure and temperature and cloud amount. A revised algorithm may soon be available from the University of Wisconsin for the GOES I-M series.

The data preparation for the dwell-sounding channel data is essentially the same as for image data. The satellite pixels around each LAPS grid point are averaged to

give a representative brightness temperature. In the algorithm currently under test, the clear-air brightness temperatures are estimated using the forward radiance computation utilizing the sounding (derived from the LAPS three-dimensional temperature and specific humidity analyses). If this approach proves too noisy, we can obtain clear-air brightness temperatures by analyzing brightness temperatures observed by GOES' clear fields-of-view.

Slicing algorithm output will be compared through both case studies and real-time study to ascertain value added. If sufficient grounds for including the technique as part of LAPS are found, cloud-top assignment from the slicing technique will be utilized in conjunction with the current window channel/sounding temperature approach. Derived cloud amount will be combined with SAO and pilot report (PIREP) data to help both quality control and expand the existing database for this aspect of cloud measurement.

In the event that cloud tops from the CO_2 slicing method are viable, the deletion process (Section 5b) can instead be carried out by comparing the heights of SAO and aircraft analyzed cloud layers to the satellite cloud top. If a given level has clouds in the initial analysis step using the SAO and aircraft data and is higher than the satellite cloud top, it is set to a cloud cover of zero.

b. *Cloud-top phase information derived from satellite data*

The 3.9 μm satellite data can possibly be used for diagnosing cloud-top water phase. The Advanced Visualization System (AVS) has been used for this research and is very powerful for image and signal processing studies. One nighttime period has been studied in which the numerical difference between the brightness counts for 3.9 μm and 11.24 μm data was formulated for an entire image. A variety of smoothing techniques were applied prior to the differencing to compensate for differing spatial resolutions. Although the result had reasonable structure (i.e., cirrus clouds and cold cloud tops mostly had small differences suggesting all ice and some stratus clouds had large differences suggesting liquid phase), the lack of ground truth made an overall assessment difficult. Furthermore, cloud-top phase identification was very much dependent on the difference threshold. More research is required that focuses on the differencing and smoothing techniques in conjunction with observations of cloud-top phase (for example, WISP-90/91 research aircraft data). It is also important to have the best cloud-top and cloud-cover analyses available, both of which require the CO_2 slicing results. Then further studies should be conducted that investigate the best technique to combine cloud cover, cloud top, visible, band 8, and 3.9 μm data in determining cloud phase.

Information about cloud-top phase can help refine vertical profiles of cloud liquid water and ice. If the satellite specifies the water/ice ratio at cloud top, we can calculate residuals at cloud top based on the existing vertical profiles of liquid and ice within LAPS. These profiles can be corrected by blending in the residuals throughout the depth of the cloud.

11. Summary

This report describes in detail how LAPS analyses of clouds and hydrometeors are performed. These analyses feed into many other segments of LAPS; for example, cloud cover feeds into the humidity analysis. Visible satellite albedo and precipitation accumulation both feed into the soil moisture analysis. Low-level cloud cover is used as part of the surface visibility analysis. Hydrometeor concentration diagnoses also feed into the CSU-RAMS forecast model. The cloud fraction analysis can be used to estimate the optical depth of cloud layers, thus helping to assess the radiation characteristics of the atmosphere in three-dimensions.

Cloud cover, rain/snow accumulation and precipitation type are useful fields to display on meteorological workstations (e.g., FSL's Dissemination Workstation) as they provide more complete nowcasting information describing surface weather conditions at any given location in the region. FSL is experimenting with a workstation for forecasters, the WFO-Advanced, that can display the three-dimensional cloud and precipitation fields. The LAPS system is a valuable test bed for utilizing many new data sources to provide a coherent picture of what the atmosphere is doing on scales of 10-100 km. During the 1990s, LAPS will continue to improve and evolve into a system that will better serve operational meteorologists.

12. References

Albers S. 1992: Photometric correction of GOES visible satellite images. *Preprints, 6th Conf. on Satellite Meteorology and Oceanography*, Atlanta, GA, Amer. Meteor. Soc., 223-225.

Albers S. 1995: The LAPS wind analysis. *Wea. Forecasting*, **10**, 342-352.

Barnes, S. L., 1964: A technique for maximizing details in numerical weather map analysis. *J. Appl. Meteor.*, **3**, 396-409.

Bleck, R., and S. G. Benjamin, 1993: Regional weather prediction with a model combining terrain-following and isentropic coordinates. Part I: model description. *Mon. Wea. Rev.*, **121**, 1770-1785.

Cram, J., and S. Albers, 1994: The use of meso-beta scale analyzed cloud cover to initialize a numerical model. *Preprints, 5th Conf. on Mesoscale Processes*, Portland, OR, Amer. Meteor. Soc., J10-J14.

Cram, J., S. Albers, M. Jackson, and J. Smart, 1995a: Three recent moisture-related analyses and modeling studies in LAPS. *WMO International Workshop on Imbalances of Slowly Varying Components of Predictable Atmospheric Motions*, Beijing, China, 7-10 March 1995.

Cram, J., S. Albers, D. Birkenheuer, J. Smart, and P. Stamus, 1995b: Meso-beta-scale assimilation in LAPS. *Preprints of the International Symposium on Assimilation of Observations in Meteorology and Oceanography*, Tokyo, Japan, 13-17 March 1995.

Donaldson, R., R. Dyer, and M. Kraus, 1975: An objective evaluator of techniques for prediction of severe weather events. *Preprints, 9th Conf. on Severe Local Storms*, Norman, OK, Amer. Meteor. Soc., 321-326.

Haines, P. A., J. K. Luers, and C. A. Cerbus, 1989: The role of the Smith-Feddes model in improving the forecasting of aircraft icing. *Preprints, 3rd Conf on the Aviation Weather System*, Anaheim, Cal, Amer. Meteor. Soc., 258-263.

Hamill, T.M., R.P. d'Entremont, and J.T. Bunting 1992: A description of the Air Force real-time nephanalysis model. *Wea. Forecasting*, **7**, 288-307.

Lipschutz, R.C., E.N. Rasmussen, J.K. Smith, J.F. Pratte, and C.R. Windsor, 1989: PROFS' 1988 real-time Doppler products subsystem. *Preprints, 24th Conf. on Radar Meteorology*, Tallahassee, FL, Amer. Meteor. Soc., 211-215.

Mahoney, J.L., C. Hartsough, P.A. Miller, M.M. Cairns, R.J. Miller, 1995: A second evaluation of avaition-impact variables generated by LAPS. NOAA Tech. Memo. ERL FSL - 16, Forecast Systems Laboratory, Boulder, CO, 89 pp.

McGinley J., and S. Albers 1991: Validation of liquid cloud water forecasts from the Smith-Feddes method derived from soundings and LAPS analyses. *Preprints, 4th International Conf. on Aviation Weather Systems*, Paris, France, Amer. Meteor.

Soc., 228-233.

McGinley J., Albers S., and P. Stamus 1991: Validation of a composite convective index as defined by a real-time local analysis system. *Wea. Forecasting*, **6**, 337-356.

McGinley, J. A., 1995: Opportunities for high resolution data analysis, prediction, and product dissemination within the local weather office. *Preprints, 14th Conf. on Weather Analysis and Forecasting*, Dallas, TX, Amer. Meteor. Soc., 478-485.

NEXRAD, 1985: Next generation weather radar algorithm report: NEXRAD Joint System Program Office, Silver Spring, Maryland.

Rasmussen, R., M. Politovich, J. Marwitz, W. Sand, J. McGinley, J. Smart, R. Pielke, S. Rutledge, D. Wesley, G. Stossmeister, B. Bernstein, K. Elmore, N. Powell, E. Westwater, B.B. Stankov, and D. Burrows, 1991: Winter Icing and Storms Project (WISP). *Bull. Amer. Meteor. Soc.*, **73**, 951-974.

Schiffer, R.A., and W. Rossow, 1985: ISSCP global radiance dataset: A new resource for climate research. *Bull. Amer. Meteor. Soc.*, **66**, 1498-1505.

Wylie, D., and P. Menzel, 1989: Two years of cloud cover statistics using VAS. *J. Climate. Appl. Meteor.*, **2**, 380-392.

Tables and Figures

Fig. 1. Three-dimensional rendition of LAPS cloud analysis showing isosurfaces of cloud cover values of 0.65.

Fig. 2. Vertical cross section through the LAPS domain showing temperature on 21 June 1995 at 1300 UTC ($0°C$).

Fig. 3. Flow diagram of data sources and sequence of events in producing LAPS three-dimensional cloud analysis. Solid lines indicate the data flow in the operational analysis, dashed lines show how the CO_2 slicing method could be implemented.

Fig. 4. Vertical cross section through the LAPS domain showing cloud cover on 2 September 1994 at 0600 UTC. Cloud cover is shown in eighths for each grid volume contained in the cross section.

Fig. 5. Schematic diagram illustrating the contributions of the various data sources in the LAPS cloud analysis.

Fig. 6. Flow diagram of fields derived primarily from the LAPS three-dimensional cloud cover analysis.

Fig. 7. Scatter plot of LAPS liquid water content vs. WISP aircraft data during an ensemble of flights in 1990. Liquid water content is shown in both axes as g m^{-3}.

Fig. 8. Plot of surface precipitation type on 14 February 1995 at 2100 UTC. The Colorado LAPS domain is shown. Precipitation type is depicted at every other grid point. Rain, freezing rain, and snow are shown by the symbols "R", "Z", and "*", respectively. Locations of SAO and mesonet stations are denoted by crosses.

Fig. 9. Plot of 5-hour precipitation accumulation on 21 June 1995 ending at 2300 UTC. The Colorado LAPS domain is shown. Liquid equivalent precipitation accumulation is contoured at .05, .10, .20, .50, and 1.00 inches. English units are used here for the convenience of forecasters in the United States.

Tables and Figures (see following pages...)

Table 1. Cloud type and drop-size specification

Ambient Temp (^{o}C)	$\frac{\partial\theta_e}{\partial z} > 0.001$	$-0.001 < \frac{\partial\theta_e}{\partial z} < 0.001$	$-0.005 < \frac{\partial\theta_e}{\partial z} < -0.001$	$\frac{\partial\theta_e}{\partial z} < -0.005$
> -10	ST–12 μm	SC–10 μm	CU–18 μm	CU/CB–25 μm (> 5 km deep)
	$\frac{\partial\theta_e}{\partial z} > 0$	$\frac{\partial\theta_e}{\partial z} < 0$		
-10 to -20	AS–10 μm	AC–18 μm		
	$\frac{\partial\theta_e}{\partial z} > 0.0005$	$-0.0005 < \frac{\partial\theta_e}{\partial z} < 0.0005$	$\frac{\partial\theta_e}{\partial z} < -0.0005$	
< -20	CS–10 μm	CI–10 μm	CC–10 μm	

ST - stratus, SC - stratocumulus, CU - cumulus, CB - cumulonimbus, AS - altostratus, AC - altocumulus, CS - cirrostratus, CI - cirrus, CC - cirrocumulus

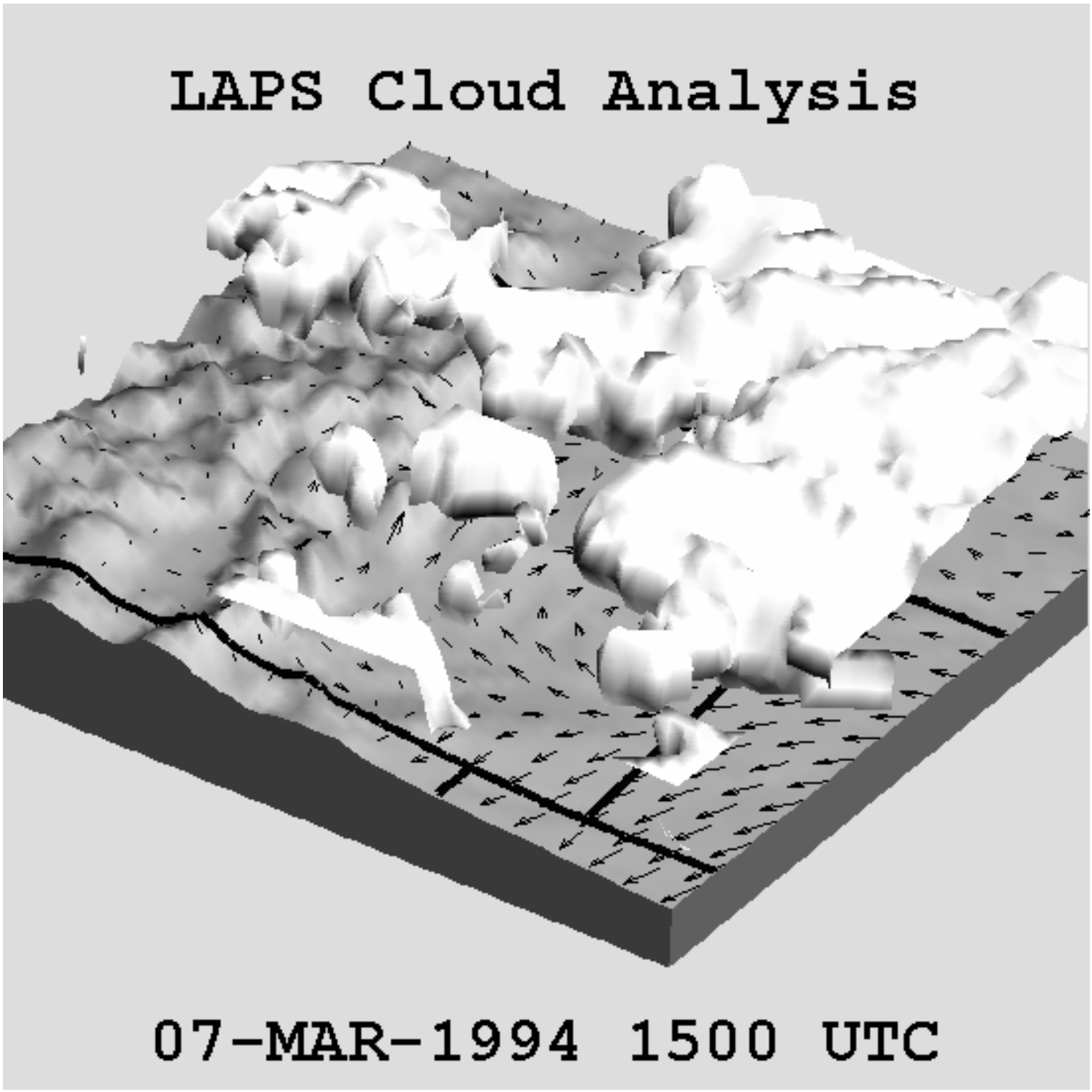

Fig. 1. Three-dimensional rendition of LAPS cloud analysis showing isosurfaces of cloud cover values of 0.65.

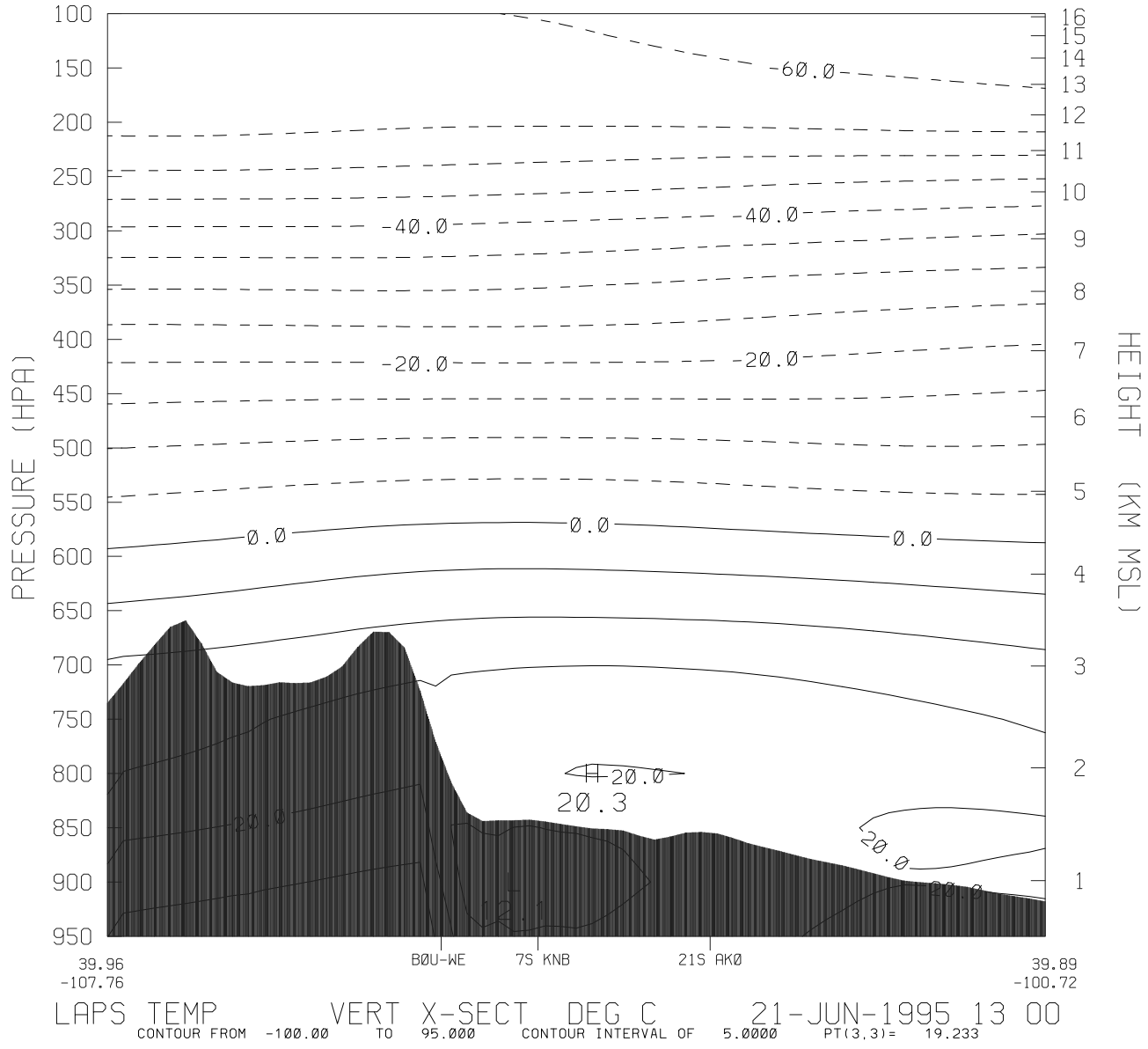

Fig. 2. Vertical cross section through the LAPS domain showing temperature on 21 June 1995 at 1300 UTC ($0°C$).

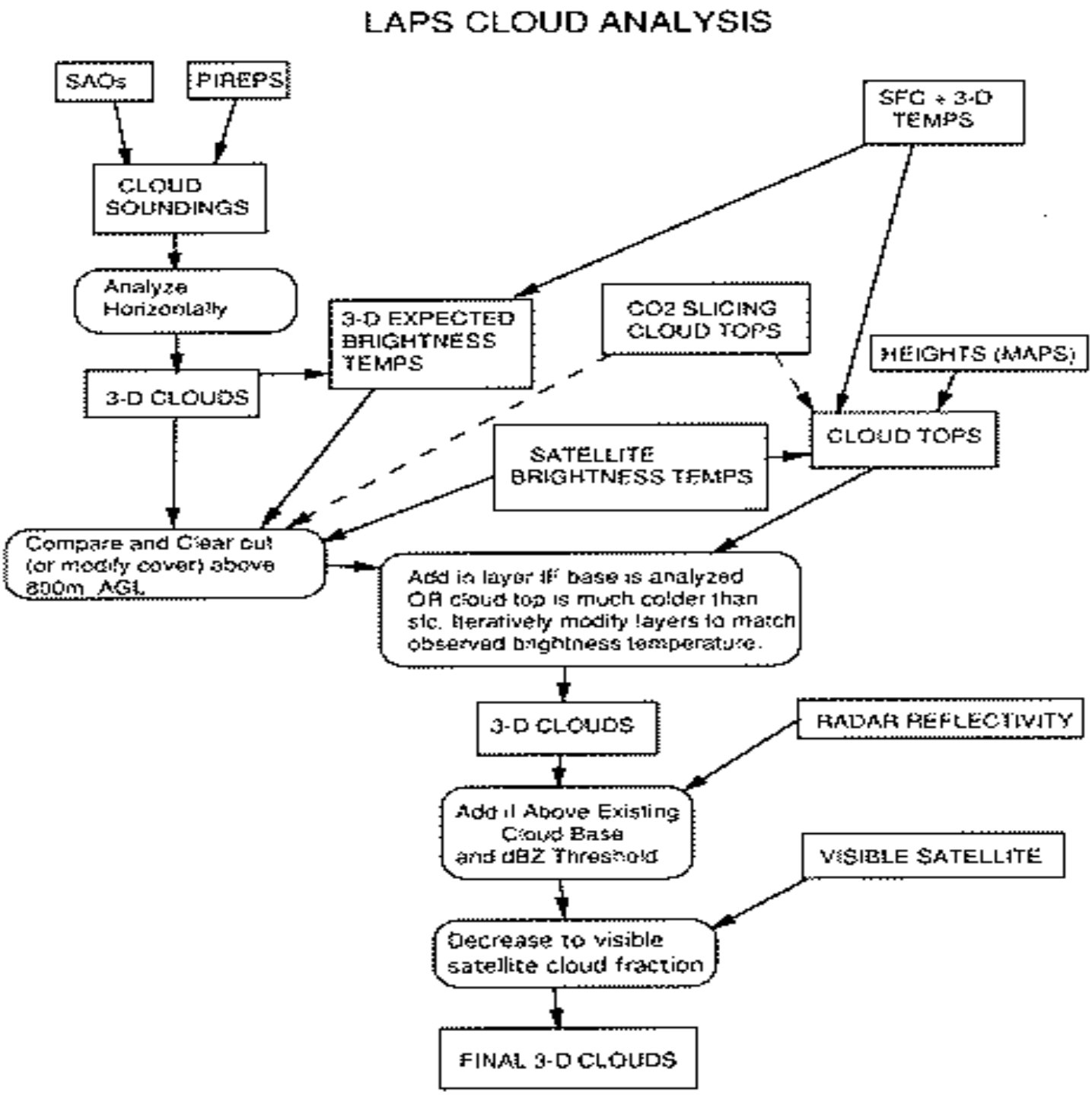

Fig. 3. Flow diagram of data sources and sequence of events in producing LAPS three-dimensional cloud analysis. Solid lines indicate the data flow in the operational analysis, dashed lines show how the CO_2 slicing method could be implemented.

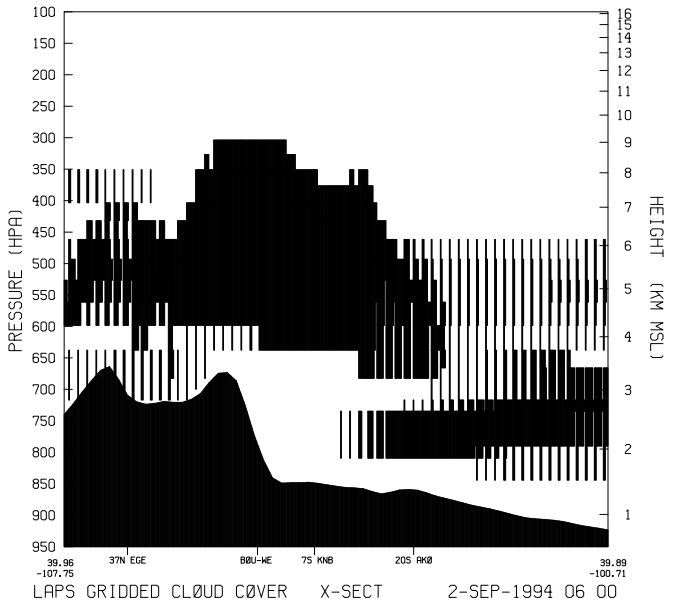

Fig. 4. Vertical cross section through the LAPS domain showing cloud cover on 2 September 1994 at 0600 UTC. Cloud cover is shown in eighths for each grid volume contained in the cross section.

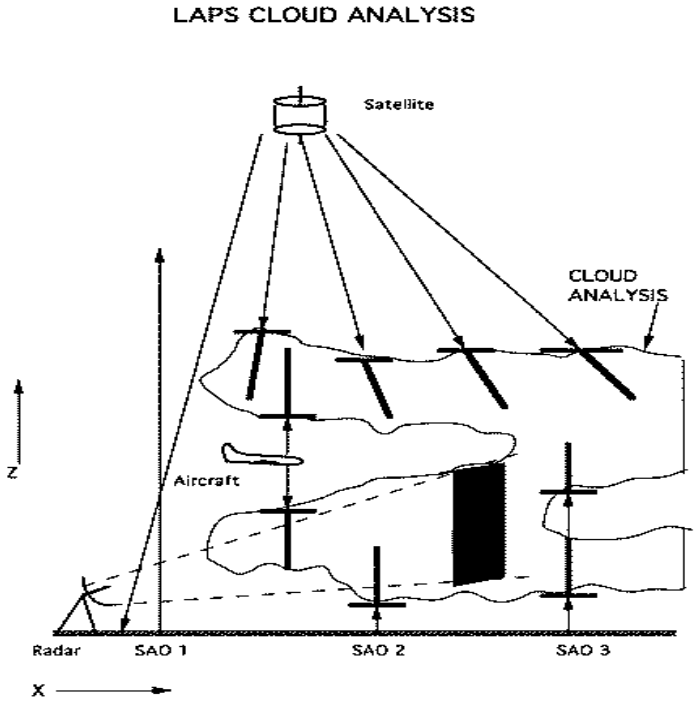

Fig. 5. Schematic diagram illustrating the contributions of the various data sources in the LAPS cloud analysis.

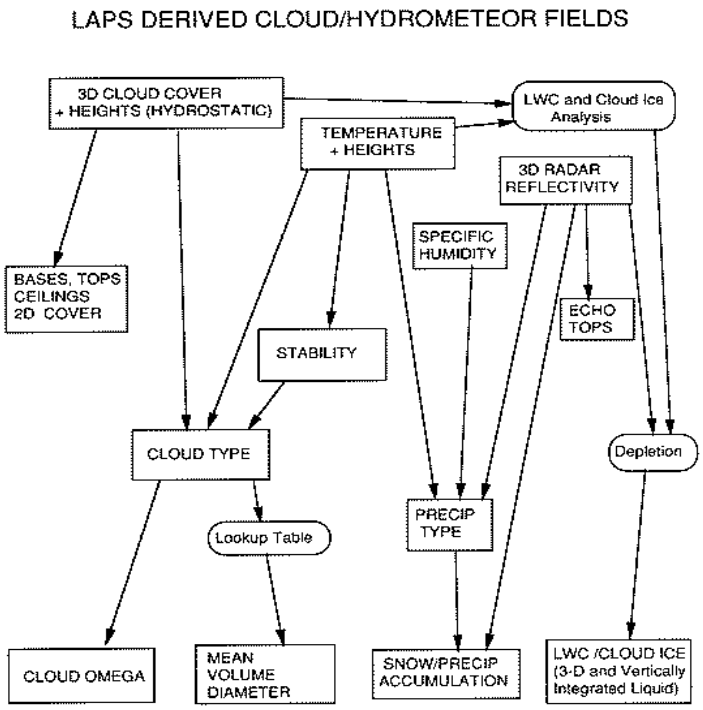

Fig. 6. Flow diagram of fields derived primarily from the LAPS three-dimensional cloud cover analysis.

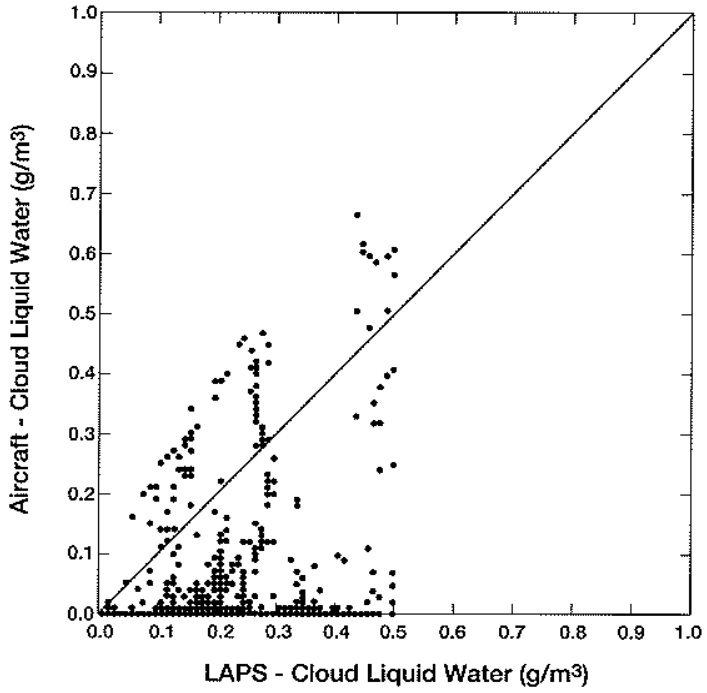

Fig. 7. Scatter plot of LAPS liquid water content vs. WISP aircraft data during an ensemble of flights in 1990. Liquid water content is shown in both axes as g m^{-3}.

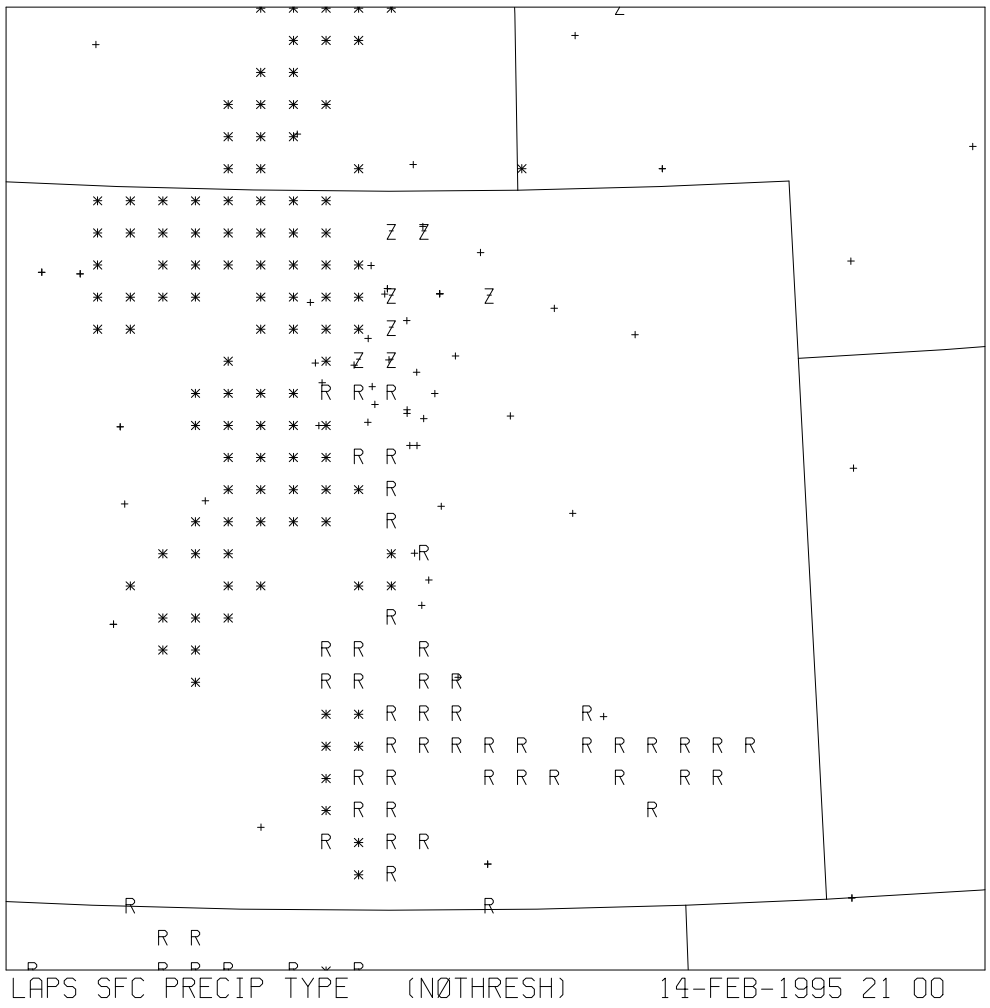

Fig. 8. Plot of surface precipitation type on 14 February 1995 at 2100 UTC. The Colorado LAPS domain is shown. Precipitation type is depicted at every other grid point. Rain, freezing rain, and snow are shown by the symbols "R", "Z", and "*", respectively. Locations of SAO and mesonet stations are denoted by crosses.

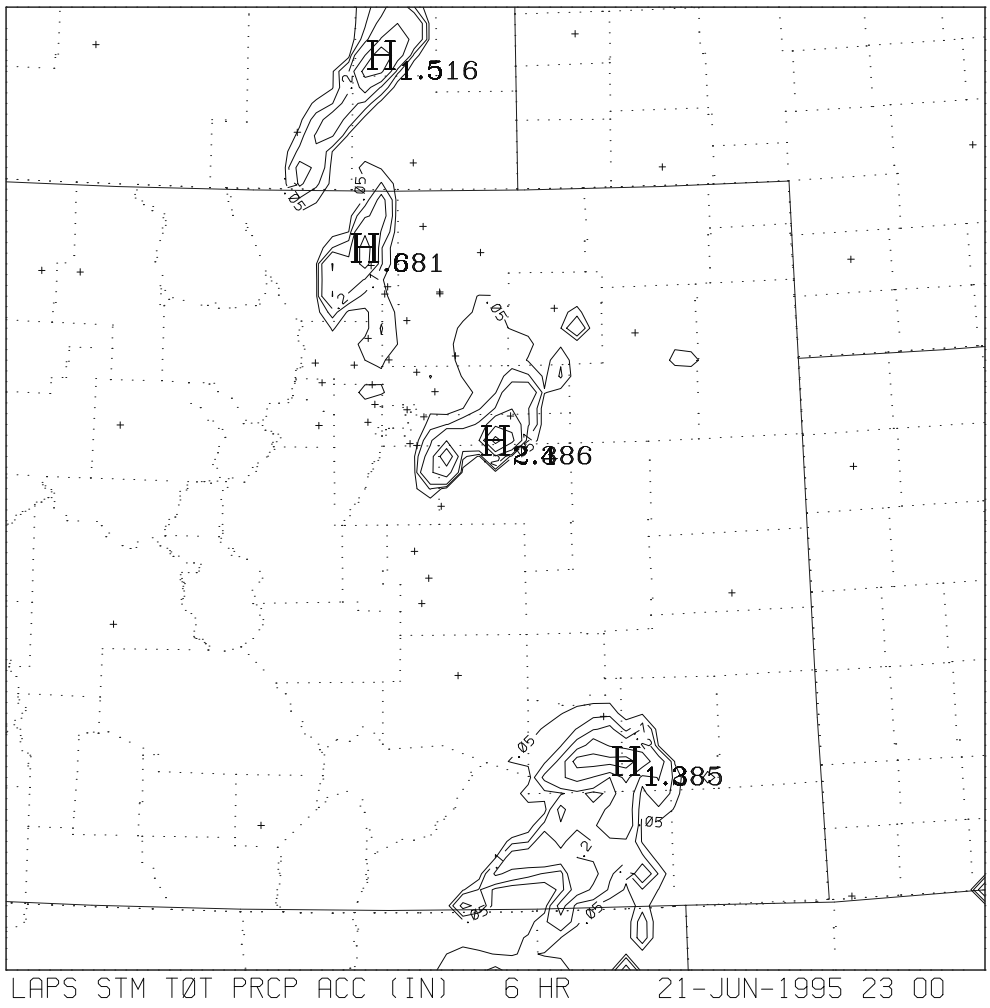

Fig. 9. Plot of 5-hour precipitation accumulation on 21 June 1995 ending at 2300 UTC. The Colorado LAPS domain is shown. Liquid equivalent precipitation accumulation is contoured at .05, .10, .20, .50, and 1.00 inches. English units are used here for the convenience of forecasters in the United States.